J. Appl. Comput. Mech., 7(1) (2021) 69-77
DOI: 10.22055/JACM.2020.34730.2470

ISSN: 2383-4536
jacm.scu.ac.ir

Shahid Chamran University of Ahvaz

Journal of Applied and Computational Mechanics

Research Paper

The Integrated Analysis of Vibrations of Quartz Crystal Plates through Artificial Coupling Factors

Qi Huang[1,2], Rongxing Wu[3], Longtao Xie[1], Jianke Du[1], Ji Wang[1]

[1] Piezoelectric Device Laboratory, School of Mechanical Engineering and Mechanics, Ningbo University, 818 FengHua Road, Ningbo, 315211 Zhejiang, China, Email: wangji@nbu.edu.cn

[2] Department of Architectural Engineering, Huzhou Vocational & Technical College, 299 Xuefu Road, Huzhou, 313000 Zhejiang, China, Email: tthq@163.com

[3] Department of Architectural Engineering, Ningbo Polytechnic, 1069 Xinda Road, Ningbo, 315800 Zhejiang, China, Email: wurongxing98@163.com

Received August 24 2020; Revised September 15 2020; Accepted for publication September 15 2020.
Corresponding author: Ji Wang (wangji@nbu.edu.cn)

Abstract. We introduce smaller artificial factors into the elastic constants matrix and manage to make Mindlin first-order plate theoryequations of motions coupled for a uniform and integrated analysis. The energy distributions of the five coupled modes are obtained and all the five vibration modes are identified through the energy calculation. This analytical approach based on artificial couplings of vibration modes suggests that all vibration modes of structural components can be analyzed through the same procedure and computer code if the right elastic constants are modified and the mode identification can be done with the energy method. This is a new technique to study multimode vibrations of structures in a broad frequency range with just one procedure and calculation tool for simplification.

Keywords: Vibration; Resonator; Quartz; Crystal; Plate; Coupling.

1. Introduction

It is known that the first-order Mindlin plate theory is widely used as the fundamental theory for the analysis of high frequency vibrations of quartz crystal resonators. Moreover, material characteristics of quartz crystal has a great impact in the resonator behaviors[1, 2]. Utilizing the Mindlin first-order plate theory [3] to study vibrations of rectangular plates of AT-cut quartz crystal is always a good choice because it can present accurate results with minimal computation costs. Theoretically, the fundamental thickness-shear (TSh) mode is only strongly coupled with the flexural (FL) mode and face-shear (FS) mode while the other two modes, the extension (EX) and thickness-twist (TT) modes, are not coupled with them. So, even there are five modes in the fundamental vibrations of the quartz crystal plates, only three modes or even two are actually taken into account in the vibration analysis.

The first-order Mindlin plate theory is widely used in the analysis of quartz crystal resonators with plate models. Mindlin analyzed the free vibrations of the AT-cut quartz crystal plate with the electric field and mass of electrode coatings using the three-mode equations and obtained useful results [4]. Lee et al. used the first-order Mindlin plate equations to solve forced vibrations of an AT-cut plate with electrodes and found results agree well with that from the three-dimensional equations [5]. Yong et al. studied both the AT- and SC-cut quartz plates and analyzed the accuracy of the plate theories of different orders [6]. The two-dimensional equations can be further simplified to one-dimensional by considering the straight-crested waves. Wang and Momosaki use the one-dimensional equations to study the forced vibrations of piezoelectric AT-cut quartz strip resonators with seven-mode model and results are in good agreement with experimental data [7]. Wang and Zhao studied the first-order Mindlin plate equations and found the technique to determinate the optimal length for resonator blanks [8].

In summary, there are three analytical models of AT-cut quartz crystal plate with the first-order Mindlin plate theory: 1) TSh and FL modes, 2) TSh, FL, and FS modes, and 3) TSh, FL, FS, EX, and TT modes. To predict the simple thickness-shear frequency [9-12], it is accurate enough to choose one of these models and calculate with the correction factors [13]. In the calculations we will obtain the frequency spectrum of vibration modes and then we need to identify each of them [8]. The design objective is always to locate the strong thickness-shear mode from the coupled spurious modes with proper resonator configurations.

Typically, the mode shapes [14, 15] are identified from the spatial distribution of displacements of each vibration mode. But this identification method is based on visualization technique which means it relies on the manual intervention and will affect the calculation efficiency. To improve this procedure, we turned to the vibration energies [16, 17] eg. stain energy[18] which can also characterize the vibration properties and are much easier for quantitative comparison. Using the energy solutions, we obtained results of identified vibration modes with the first-order Mindlin plate theory [19]. In the numerical examples earlier, we can only use three modes model as mentioned before to calculate the energy distributions, simply because the TSh, FL, and FS modes are not coupled with EX and TT modes [3], and their displacements cannot be calculated from the same procedure. Therefore, the total energy has to be artificially divided into two parts for each group of modes. Calculations with separated groups of vibration modes are slow and incomparable. In particular, the incomplete calculation of vibration modes will break the solution consistency comparing with the FEM solutions [20-22]. In this paper, we present a procedure to enable the five vibration modes in the first-order Mindlin plate theory to be coupled by using artificial elastic constants. Artificial modification is sometimes proved effective through solving equations with some mandatory purposes [23]. As a result, we manage to calculate vibration modes with the energy solution and succeed in identifying vibration modes accurately. We believe this method and procedure is a new technique in the vibrations analysis of quartz crystal plates with practical importance. In addition, the artificial couplings introduced in this study can be used in occasions with multimode vibrations in a wide frequency range for simplified analysis with just one procedure and calculation tool.

2. Equations of the First-Order Mindlin Plate Theory

For the vibration analysis of AT-cut quartz crystal plates with the first-order Mindlin plate theory, there are six components of displacements. The flexure $u_2^{(0)}$, face-shear $u_3^{(0)}$, and thickness-shear $u_1^{(1)}$ modes are strongly coupled. The displacements $u_1^{(0)}$ and $u_3^{(1)}$ are the extensional and thickness-twist mode which are only coupled with themselves. The thickness-stretch mode $u_2^{(1)}$ is solved as a known variable for approximate consideration in an AT-cut quartz crystal plate and it can be expressed by other displacements [3]. As a result, there are five vibration modes in the first-order Mindlin plate theory of an AT-cut plate. The calculation model of rectangle AT-cut quartz crystal plate is shown in Fig. 1 with a rotation of 35.25° along the crystal axis.

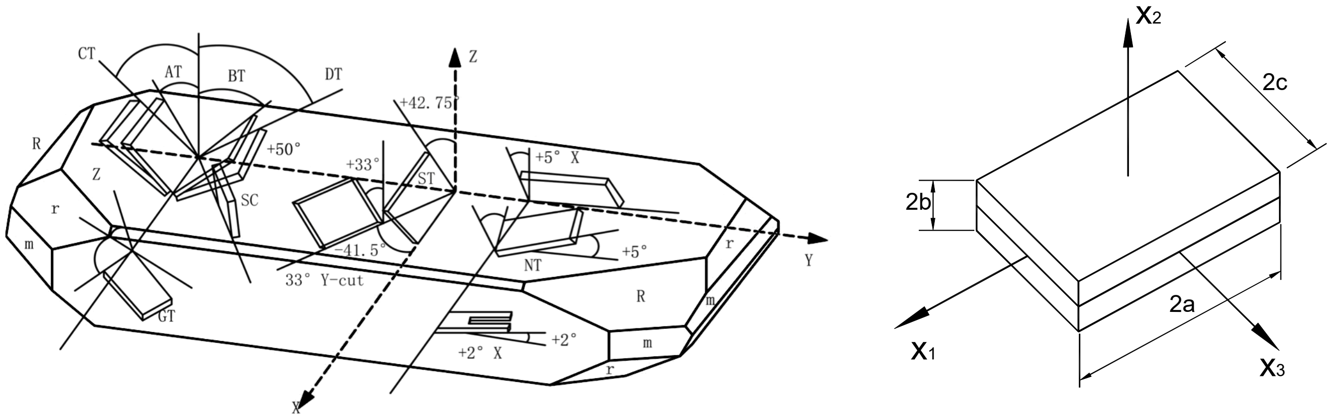

(a) Orientation of cuts of quartz crystal (b) A resonator model

Fig. 1. AT-cut rectangle quartz crystal resonator model.

2.1 The five-mode equations with artificial coupling factors

The stress-displacements relations of the first-order Mindlin plate equation of AT-cut quartz crystal with the full matrix of elastic constants are [3]

$$
\begin{aligned}
T_1^{(0)} &= 2b\left[c_{11}u_{1,1}^{(0)} + \kappa_4 c_{14}u_3^{(1)} + c_{15}u_{3,1}^{(0)} + \kappa_6 c_{16}\left(u_{2,1}^{(0)} + u_1^{(1)}\right)\right],\\
T_3^{(0)} &= 2b\left[c_{31}u_{1,1}^{(0)} + \kappa_4 c_{34}u_3^{(1)} + c_{35}u_{3,1}^{(0)} + \kappa_6 c_{36}\left(u_{2,1}^{(0)} + u_1^{(1)}\right)\right],\\
T_4^{(0)} &= 2\kappa_4 b\left[c_{41}u_{1,1}^{(0)} + \kappa_4 c_{44}u_3^{(1)} + c_{45}u_{3,1}^{(0)} + \kappa_6 c_{46}\left(u_{2,1}^{(0)} + u_1^{(1)}\right)\right],\\
T_5^{(0)} &= 2b\left[c_{51}u_{1,1}^{(0)} + \kappa_4 c_{54}u_3^{(1)} + c_{55}u_{3,1}^{(0)} + \kappa_6 c_{56}\left(u_{2,1}^{(0)} + u_1^{(1)}\right)\right],\\
T_6^{(0)} &= 2\kappa_6 b\left[c_{61}u_{1,1}^{(0)} + \kappa_4 c_{64}u_3^{(1)} + c_{65}u_{3,1}^{(0)} + \kappa_6 c_{66}\left(u_{2,1}^{(0)} + u_1^{(1)}\right)\right],\\
T_1^{(1)} &= \frac{2b^3}{3}\left[\bar{c}_{11}u_{1,1}^{(1)} + \bar{c}_{15}u_{3,1}^{(1)}\right],\\
T_3^{(1)} &= \frac{2b^3}{3}\left[\bar{c}_{31}u_{1,1}^{(1)} + \bar{c}_{35}u_{3,1}^{(1)}\right],\\
T_5^{(1)} &= \frac{2b^3}{3}\left[\bar{c}_{51}u_{1,1}^{(1)} + \bar{c}_{55}u_{3,1}^{(1)}\right],\\
\bar{c}_{ij} &= c_{ij} - \frac{c_{i2}c_{2i}}{c_{22}}, i, j = 1,3,4,
\end{aligned}
\tag{1}
$$

where the $T_p^{(0)}(p=1,3,4,5,6)$, $T_p^{(1)}(p=1,3,5)$, $u_j^{(0)}(j=1,2,3)$, $u_j^{(1)}(j=1,3)$, and b are the zeroth-order stress, first-order stress, zeroth-order displacement, first-order displacement, and half of plate thickness in Fig. 1, respectively. The $c_{ij}(i,j=1,2,3,4,5,6)$ are the elastic constants [24], and $\bar{c}_{ij}$, are the modified elastic constants after the truncation of the plate equations. The κ_4 and κ_6 are the correction factors for the first-order Mindlin plate theory as

$$\kappa_4 = \kappa_6 = \sqrt{\frac{\pi^2}{12}}, \tag{2}$$

Then the first-order equations of motion are [3]

$$
\begin{aligned}
&T_{1,1}^{(0)} + T_{5,3}^{(0)} = 2b\rho\ddot{u}_1^{(0)},\\
&T_{6,1}^{(0)} + T_{4,3}^{(0)} = 2b\rho\ddot{u}_2^{(0)},\\
&T_{5,1}^{(0)} + T_{3,3}^{(0)} = 2b\rho\ddot{u}_3^{(0)},\\
&T_{1,1}^{(1)} + T_{5,3}^{(1)} - T_{6}^{(0)} = \frac{2b^3}{3}\rho\ddot{u}_1^{(1)},\\
&T_{5,1}^{(1)} + T_{3,3}^{(1)} - T_{4}^{(0)} = \frac{2b^3}{3}\rho\ddot{u}_3^{(1)},
\end{aligned}
\tag{3}
$$

where ρ is the density of quartz crystal. To study the thickness-shear vibrations, we define displacement expressions of the five modes, according to the assumption of straight-crested waves along the x_1 axis and the functioning vibration modes, as [25]

$$
\begin{aligned}
&u_1^{(0)} = A_1 \sin\xi x_1 e^{i\omega t},\\
&u_2^{(0)} = A_2 \sin\xi x_1 e^{i\omega t},\\
&u_3^{(0)} = A_3 \sin\xi x_1 e^{i\omega t},\\
&u_1^{(1)} = \frac{A_4}{b}\cos\xi x_1 e^{i\omega t},\\
&u_3^{(1)} = \frac{A_5}{b}\cos\xi x_1 e^{i\omega t},
\end{aligned}
\tag{4}
$$

where $A_j\,(j=1,2,3,4,5)$, ξ, ω and t are the vibration amplitudes, wavenumber, frequency, and time, respectively.

With the consideration of the zeroes of elastic constants of AT-cut quartz crystal, then substituting Eqs. (1) and (2) into eq. (3), we obtain the determinant equation of the coefficients of dispersion relations as

$$
\begin{vmatrix}
\frac{c_{11}}{c_{66}}Z^2-\Omega^2 & 0 & 0 & 0 & \frac{c_{14}}{c_{66}}\kappa_4\frac{2}{\pi}Z\\
0 & \frac{\pi^2}{12}Z^2-\Omega^2 & \frac{c_{65}}{c_{66}}\frac{\pi}{2\sqrt{3}}Z^2 & \frac{\pi}{6}Z & 0\\
0 & \frac{c_{56}}{c_{66}}\frac{\pi}{2\sqrt{3}}Z^2 & \frac{c_{55}}{c_{66}}Z^2-\Omega^2 & \frac{c_{56}}{c_{66}}\frac{Z}{\sqrt{3}} & 0\\
0 & \kappa_6\frac{\pi}{2}Z & \frac{c_{65}}{c_{66}}\frac{\pi}{2}Z & \frac{\bar{c}_{11}}{c_{66}}\kappa_6 Z^2+\kappa_6-\kappa_6\Omega^2 & 0\\
\frac{c_{41}}{c_{66}}\frac{\pi}{2}Z & 0 & 0 & 0 & \frac{\bar{c}_{55}}{c_{66}}\kappa_4 Z^2+\frac{c_{44}}{c_{66}}\kappa_6-\kappa_4\Omega^2
\end{vmatrix} = 0,
\tag{5}
$$

where Z , and Ω are the normalized wavenumber and frequency with definitions as

$$
Z = \frac{\xi}{\frac{\pi}{2b}}, \Omega = \frac{\omega}{\omega_0}, \omega_0 = \frac{\pi}{2b}\sqrt{\frac{c_{66}}{\rho}},
\tag{6}
$$

where ω_0 is the frequency of the fundamental thickness-shear mode.

By solving the eq. (5) we can obtain the displacements expressions as

$$
\begin{aligned}
&u_j^{(0)} = \sum_{i=1}^{5} A_{4i}\alpha_{ji}\sin\left(\frac{\pi Z_i}{2}\frac{x_i}{b}\right)e^{i\omega t}, j=1,2,3,\\
&u_j^{(1)} = \sum_{i=1}^{5} \frac{A_{4i}}{b}\alpha_{ji}\cos\left(\frac{\pi Z_i}{2}\frac{x_i}{b}\right)e^{i\omega t}, j=1,3,
\end{aligned}
\tag{7}
$$

where $Z_j\,(j=1,2,3,4,5)$, $A_{4j}\,(j=1,2,3,4,5)$, and $\alpha_{ij}\,(i,j=1,2,3,4,5)$ are the jth wavenumber, vibration amplitudes of thickness-shear mode at jth wavenumber, and amplitudes ratios which defined as:

$$
\alpha_{ji} = \frac{A_{ij}}{A_{4i}}, i,j = 1,2,3,4,5.
\tag{8}
$$

The problem is that we cannot obtain reasonable values of α_{ij} in eq. (7) from the eq. (5) since the equations are not coupled. We can see form the eq. (5) that the five modes are not coupled due to the absence of some elastic constants of the AT-cut quartz crystal. This is not necessarily a good situation if we want to use the computer code based on the five mode for the analysis, because the code has to be reconfigured with less equations and solve separately for certain materials. Then, it is natural to ask if we can use the same code for all equations to be solved without breaking them into small groups to reduce the time and modification of the code. Clearly, if we modify the elastic matrix by changing some constants to nonzero to establish the couplings, we may manage to make the equations coupled for a one-stop solution with the same code and procedure. By observing the elastic constants and the equations of motion Eqs. (1) and (3), we find the parameters c_{15} and c_{16} are the good choices for modifying and as we should know the AT-cut crystal is monoclinic so the elastic constants are diagonally symmetric thus c_{51} and c_{61} are also changed. In the following calculations we will set the c_{15} and c_{16} to a small value ε and modify the dispersion equations.

We let $c_{15}=c_{51}=\varepsilon, c_{16}=c_{61}=0$ or $c_{15}=c_{51}=0, c_{16}=c_{61}=\varepsilon$ and the eq. (5) now become as

$$\begin{vmatrix} \frac{c_{11}}{c_{66}}Z^2-\Omega^2 & \frac{c_{16}}{c_{66}}\kappa_6 Z^2 & \frac{c_{15}}{c_{66}}Z^2 & \frac{c_{16}}{c_{66}}\kappa_6\frac{2}{\pi}Z & \frac{c_{14}}{c_{66}}\kappa_4\frac{2}{\pi}Z \\ \frac{c_{61}}{c_{66}}\kappa_6 Z^2 & \frac{\pi^2}{12}Z^2-\Omega^2 & \frac{c_{65}}{c_{66}}\frac{\pi}{2\sqrt{3}}Z^2 & \frac{\pi}{6}Z & 0 \\ \frac{c_{51}}{c_{66}}Z^2 & \frac{c_{56}}{c_{66}}\frac{\pi}{2\sqrt{3}}Z^2 & \frac{c_{55}}{c_{66}}Z^2-\Omega^2 & \frac{c_{56}}{c_{66}}\frac{Z}{\sqrt{3}} & 0 \\ \frac{c_{61}}{c_{66}}\frac{\pi}{2}Z & \kappa_6\frac{\pi}{2}Z & \frac{c_{65}}{c_{66}}\frac{\pi}{2}Z & \frac{\bar{c}_{11}}{c_{66}}\kappa_6 Z^2+\kappa_6-\kappa_6\Omega^2 & \frac{\bar{c}_{15}}{c_{66}}\kappa_6 Z^2 \\ \frac{c_{41}}{c_{66}}\frac{\pi}{2}Z & 0 & 0 & \frac{\bar{c}_{51}}{c_{66}}\kappa_4 Z^2 & \frac{\bar{c}_{55}}{c_{66}}\kappa_4 Z^2+\frac{c_{44}}{c_{66}}\kappa_6-\kappa_4\Omega^2 \end{vmatrix}=0. \tag{9}$$

Form the eq. (9) we can see that the new dispersion equations are well coupled for all the displacements presented in eq. (7). Finally, we substitute the eq. (9) into the boundary conditions to obtain the vibration frequency and amplitudes. The traction-free boundary conditions in this case are given as

$$T_1^{(0)}=0, T_5^{(0)}=0, T_6^{(0)}=0, T_1^{(1)}=0, T_5^{(1)}=0, x_1=\pm a. \tag{10}$$

where a is the half length of the resonator as shown in Fig. 1.

We are not going to expand the equations here, as it was discussed in many studies before [3, 8]. By solving the eq. (10) with a standard procedure we can obtain the amplitudes ratios β_r of wave-numbers of each single mode as [26],

$$\beta_r=\frac{A_{4r}}{A_{44}}, r=1,2,3,4,5. \tag{11}$$

With eq. (11), we have completed the calculation and obtained the analytical expressions of each vibration mode which can be used in energy calculation for mode identification purpose.

2.2 Vibration mode identification with the kinetic and strain energies

The vibration mode identification is very important in the analysis of vibrations of structures including quartz crystal plates. The TSh mode as the primary functioning mode is expected to be dominant near the vicinity of working frequency. There is an alternative way for mode identification with energies [19] without using the traditional mode shapes. Following the calculation procedure for the strain and kinetic energies of each mode, the distributions of energies can be used for the labeling of vibration modes. Usually the dominant vibration mode is designated as the one with the highest concentration of modal energies. The procedure is proved efficiency and reliable in the AT-cut quartz crystal model with the first-order Mindlin plate theory.

First, the strain energy density of the Mindlin plate is [3]

$$\begin{aligned}\bar{U}&=\frac{1}{2}c_{pq}\sum_m\sum_n B_{mn}S_p^{(m)}S_q^{(n)}\\ &=\frac{1}{2}B_{00}c_{11}\left(u_{1,1}^{(0)}\right)^2+\frac{1}{2}B_{00}c_{55}\left(u_{3,1}^{(0)}\right)^2+\frac{1}{2}B_{00}c_{66}\left(u_{2,1}^{(0)}\right)^2\\ &+\frac{1}{2}B_{00}c_{66}\left(u_1^{(1)}\right)^2+\frac{1}{2}B_{11}c_{11}\left(u_{1,1}^{(1)}\right)^2+\frac{1}{2}B_{00}c_{44}\left(u_3^{(1)}\right)^2+\frac{1}{2}B_{11}c_{55}\left(u_{3,1}^{(1)}\right)^2\\ &+B_{00}c_{66}u_{2,1}^{(0)}u_1^{(1)}+B_{00}c_{14}u_{1,1}^{(0)}u_3^{(1)}+B_{00}c_{15}u_{1,1}^{(0)}u_{3,1}^{(0)}\\ &+B_{00}c_{16}u_{1,1}^{(0)}u_{2,1}^{(0)}+B_{00}c_{16}u_{1,1}^{(0)}u_1^{(1)}+B_{00}c_{45}u_{3,1}^{(0)}u_3^{(1)}\\ &+B_{00}c_{56}u_{2,1}^{(0)}u_{3,1}^{(0)}+B_{00}c_{56}u_{3,1}^{(0)}u_1^{(1)}+B_{11}c_{15}u_{1,1}^{(1)}u_{3,1}^{(1)}.\end{aligned} \tag{12}$$

We can classify the energy density with their modes, like the thickness-shear (TSh) and extension (EX) modes, as

$$\begin{aligned}\bar{U}_{TSH}&=\frac{1}{2}B_{00}c_{66}\left(u_1^{(1)}\right)^2+\frac{1}{2}B_{11}c_{11}\left(u_{1,1}^{(1)}\right)^2,\\ \bar{U}_{EX}&=\frac{1}{2}B_{00}c_{11}\left(u_{1,1}^{(0)}\right)^2.\end{aligned} \tag{13}$$

Then by substituting eq. (7) into eq. (14) and integrate it over the whole plate for one period of time we can obtain the energy

$$\begin{aligned}U_{TSH}&=\int_0^{\frac{2\pi}{\omega}}\int_{-c}^{c}\int_{-a}^{a}\bar{U}_{TSH}dx_1dx_3dt\\ &=\frac{2\pi}{\omega}c_{66}\left\{\sum_{i=1}^{5}A_{4i}^2\alpha_{4i}^2\left[\frac{a}{b}+\frac{1}{\pi Z_i}\sin\left(\frac{a}{b}\pi Z_i\right)\right]+2\sum_{i=1,i\neq j}^{5}\frac{A_{4i}A_{4j}\alpha_{4i}\alpha_{4j}}{\pi}\left[\frac{\sin\left(\frac{a}{b}\frac{\pi}{2}(Z_i-Z_j)\right)}{Z_i-Z_j}+\frac{\sin\left(\frac{a}{b}\frac{\pi}{2}(Z_i+Z_j)\right)}{Z_i+Z_j}\right]\right\}\\ &+\frac{\pi^3}{6\omega}c_{11}\left\{\sum_{i=1}^{5}A_{4i}^2\alpha_{4i}^2\left[\frac{a}{b}-\frac{1}{\pi Z_i}\sin\left(\frac{a}{b}\pi Z_i\right)\right]+2\sum_{i=1,i\neq j}^{5}\frac{A_{4i}A_{4j}\alpha_{4i}\alpha_{4j}}{\pi}\left[\frac{\sin\left(\frac{a}{b}\frac{\pi}{2}(Z_i-Z_j)\right)}{Z_i-Z_j}-\frac{\sin\left(\frac{a}{b}\frac{\pi}{2}(Z_i+Z_j)\right)}{Z_i+Z_j}\right]\right\}\end{aligned} \tag{14}$$

as

$$\begin{aligned} U_{EX} &= \int_0^{\frac{2\pi}{\omega}}\int_{-c}^{c}\int_{-a}^{a}\bar{U}_{EX}\mathrm{d}x_1\mathrm{d}x_3\mathrm{d}t \\ &= \frac{2\pi}{\omega}c_{11}\left\{\sum_{i=1}^{5}A_{4i}^2\alpha_{4i}^2\left[\frac{a}{b}-\frac{1}{\pi Z_i}\sin\left(\frac{a}{b}\pi Z_i\right)\right]+2\sum_{i=1,i\neq j}^{5}\frac{A_{4i}A_{4j}\alpha_{4i}\alpha_{4j}}{\pi}\left[\frac{\sin\left(\frac{a}{b}\frac{\pi}{2}(Z_i-Z_j)\right)}{Z_i-Z_j}-\frac{\sin\left(\frac{a}{b}\frac{\pi}{2}(Z_i+Z_j)\right)}{Z_i+Z_j}\right]\right\} \end{aligned} \tag{14}$$

Following the same procedure we can obtain the kinetic energy expressions as [3],

$$\bar{K}=\frac{1}{2}\rho\sum_m\sum_n B_{mn}\dot{u}_j^{(m)}\dot{u}_j^{(n)}=\frac{1}{2}\rho\left(B_{00}\dot{u}_1^{(0)}\dot{u}_1^{(0)}+B_{00}\dot{u}_2^{(0)}\dot{u}_2^{(0)}+B_{00}\dot{u}_3^{(0)}\dot{u}_3^{(0)}+B_{11}\dot{u}_1^{(1)}\dot{u}_1^{(1)}+B_{11}\dot{u}_3^{(1)}\dot{u}_3^{(1)}\right). \tag{15}$$

$$\begin{aligned} K_{TSH} &= \int_0^{\frac{2\pi}{\omega}}\int_{-c}^{c}\int_{-a}^{a}\bar{K}_{TSH}\mathrm{d}x_1\mathrm{d}x_3\mathrm{d}t=\int_0^{\frac{2\pi}{\omega}}\int_{-c}^{c}\int_{-a}^{a}\frac{1}{2}\rho B_{11}\dot{u}_1^{(1)}\dot{u}_1^{(1)}\mathrm{d}x_1\mathrm{d}x_3\mathrm{d}t \\ &= \rho\frac{4\pi b^2 c}{3\omega}\left\{\sum_{i=1}^{5}A_{4i}^2\alpha_{4i}^2\left[\frac{a}{b}+\frac{1}{\pi Z_i}\sin\left(\frac{a}{b}\pi Z_i\right)\right]+2\sum_{i=1,i\neq j}^{5}\frac{A_{4i}A_{4j}\alpha_{4i}\alpha_{4j}}{\pi}\left[\frac{\sin\left(\frac{a}{b}\frac{\pi}{2}(Z_i-Z_j)\right)}{Z_i-Z_j}+\frac{\sin\left(\frac{a}{b}\frac{\pi}{2}(Z_i+Z_j)\right)}{Z_i+Z_j}\right]\right\}, \\ K_{EX} &= \int_0^{\frac{2\pi}{\omega}}\int_{-c}^{c}\int_{-a}^{a}\bar{K}_{EX}\mathrm{d}x_1\mathrm{d}x_3\mathrm{d}t=\int_0^{\frac{2\pi}{\omega}}\int_{-c}^{c}\int_{-a}^{a}\frac{1}{2}\rho B_{11}\dot{u}_1^{(0)}\dot{u}_1^{(0)}\mathrm{d}x_1\mathrm{d}x_3\mathrm{d}t \\ &= \rho\frac{4\pi b^2 c}{\omega}\left\{\sum_{i=1}^{5}A_{4i}^2\alpha_{4i}^2\left[\frac{a}{b}-\frac{1}{\pi Z_i}\sin\left(\frac{a}{b}\pi Z_i\right)\right]+2\sum_{i=1,i\neq j}^{5}\frac{A_{4i}A_{4j}\alpha_{4i}\alpha_{4j}}{\pi}\left[\frac{\sin\left(\frac{a}{b}\frac{\pi}{2}(Z_i-Z_j)\right)}{Z_i-Z_j}-\frac{\sin\left(\frac{a}{b}\frac{\pi}{2}(Z_i+Z_j)\right)}{Z_i+Z_j}\right]\right\}, \end{aligned} \tag{16}$$

where c represents the half width of the plate in Fig. 1.

To obtain the energy distributions, we sum up all the energies together as

$$P_Y=\begin{cases}\dfrac{U_Y}{\sum U_X}\times 100\%, & \text{for strain energy,}\\[2ex] \dfrac{K_Y}{\sum K_X}\times 100\%, & \text{for kinetic energy,}\end{cases} \tag{17}$$
$$X,Y=EX,FL,FS,TSh,TT,$$

where P_X are the percentages of the energy distribution of the specific mode. The coupled energies are omitted due to their comparatively small values.

The above results showed us the energy solution of an AT-cut quartz crystal plate with the first-order Mindlin plate theory of five modes. They cannot be calculated without the solutions from eq. (7). Clearly, the artificial factors successfully enabled the uniform implementation of the energy proportion among all modes and amplitudes for comparisons.

3. Numerical Results

In this section, numerical results of three- and five-mode models will be presented based on the energy formulation with artificial factors. The plate model is the rectangle AT-cut quartz crystal plate with four free sides, and the electrodes and piezoelectric effects are neglected.

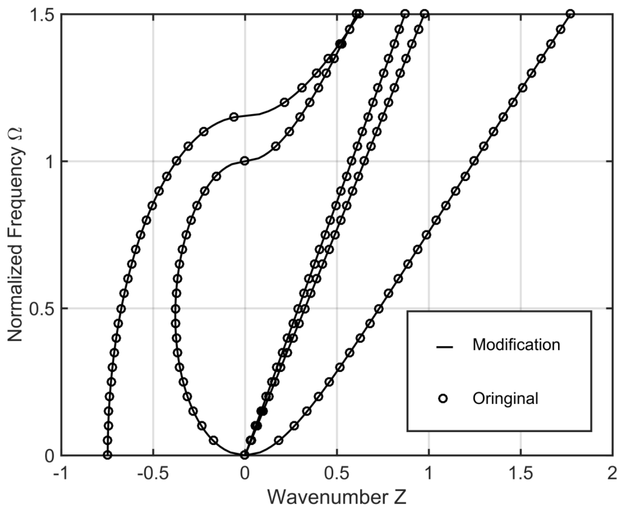

Fig. 2. Dispersion relation from the original five modes and the modified equations with $c_{16}=10^{-5}$

First, we focus on the changes of the artificial factors brought into the equations. The dispersion relations are the important feature to indicate the characteristics of vibration modes. The dispersion relation reveals the relations between the normalized wavenumber and the frequency and can also help us to find out the cut-off frequency of the specific wave mode. In this study, we use the dispersion relations to verify the modification of the equations as shown in Fig. 2. We compare the original dispersion relations with the modified equations in eq. (5) with artificial factor $c_{16} = 10^{-5}$. Figure 1 shows these two sets of dispersion curves are exactly the same, implying the equations with the artificial facts still maintain their exact characteristics.

Then we present the frequency spectra of both the three and five modes in Figs. 3 and 4. These frequency spectra will cover all the possible frequencies in a specific range, including all possible optimal working frequencies. The frequencies in Fig. 4 are more complex than the Fig. 3 because of the extra frequencies of the TT and EX mode. The optimal working modes in the spectra can be selected by the mode identification method.

The traditional identification method requires plotting displacements of each mode and relies on the assistance of visual examination. However, the energy solution approach is more efficient. The energy solution starts with calculating the energy distributions of vibration modes. From Figs. 3 and 4, we select frequency points at the specific length to thickness ratio 33.0 for calculating the strain and kinetic energy distribution of each mode.

Table 1 shows the energy distributions of the three-mode model and the high concentration of modal energy with its value in bold indicating the dominance mode prominent. We can see in the Table 1 the energy distributions of different modes are listed at the specific thickness to length ratio 33.0 and the values of the strain and kinetic energies have been showing the exactly same trend. The differences between the two energies are in their coupled parts [29], but overall both indicate the same weight for the mode identification. We can clearly identify the frequency of working mode form the Table 1 as its TSh modal energy is 98% at the 4th row.

Table 2 presents the energy distributions of the five-mode model with artificial factors $c_{15} = c_{51} = 10^{-5}$. Compared with the Table 1, Table 2 can identify two more extra modes, namely the TT and EX modes. Meanwhile, the frequency points of Table 2 are more than those in Table 1 and the extra points are from the frequency spectra brought in by the TT and EX modes. We can see from the Table 2 the characteristics of extra frequency points are obvious. The energy distribution of these points which marked with underline in the Table 2 are clear, and the value of the TT and EX modes are comparatively higher than that of the FS, FL, and TSh mode whose value are nearly zero so they clearly indicates that these frequencies belong to the TT and EX modes. It obtains almost the same conclusion as the Table 2 when the artificial factors are $c_{16} = c_{61} = 10^{-5}$. The affect of artificial factors between c_{15} and c_{16} is minimal and their numerical difference is in the order of 10^{-3}. The artificial factors have the same effect and we can choose either one of them for calculations.

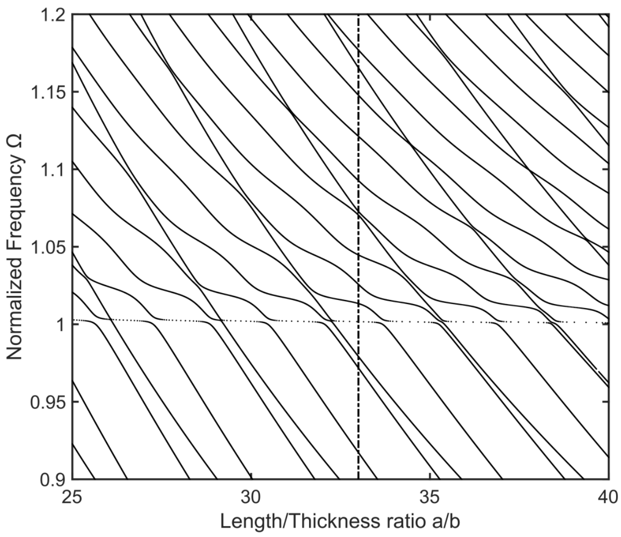

Fig. 3. Frequency versus length/thickness ratio of the coupled TSh, FS, and FL modes

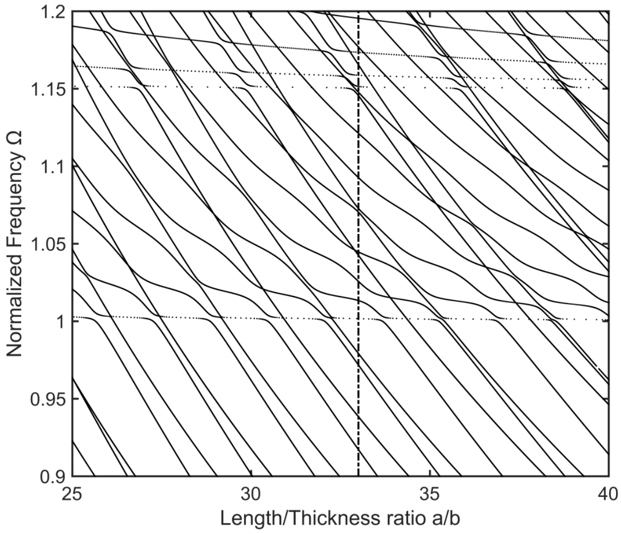

Fig. 4. Frequency versus length/thickness ratio of the coupled TT, EX, TSh, FS, and FL modes

Table 1. Strain/Kinetic(S/K) energy distributions of the crystal plate at each resonance with three vibration modes.

Mode Number	Normalized Frequency	Flexural (S/K %)	Face-shear (S/K %)	**Thickness-shear (S/K %)**
1	0.917209859	**76.4 / 88.7**	0.4 / 0.4	23.2 / 10.9
2	0.971792029	**72.5 / 79.8**	3.6 / 6.0	23.9 / 14.2
3	0.979196968	8.1 / 5.4	**89.0 / 93.7**	2.9 / 0.9
4	1.001676224	1.4 / 1.2	0.0 / 0.0	**98.6 / 98.8**
5	1.013360338	19.3 / 16.8	0.1 / 0.1	**80.6 / 83.1**
6	1.025727449	**53.9 / 53.4**	0.3 / 0.3	45.8 / 46.3
7	1.044711639	27.2 / 24.3	0.1 / 0.1	**72.6 / 75.6**
8	1.070398309	35.4 / 31.1	24.3 / 30.7	**40.3 / 38.2**
9	1.072808022	12.4 / 9.7	**62.4 / 68.4**	25.2 / 21.9
10	1.092680606	48.9 / 46.9	0.5 / 0.65	**50.7 / 52.5**
11	1.121264339	45.2 / 43.0	0.2 / 0.1	**54.6 / 56.8**
12	1.147777217	**51.3 / 49.5**	0.8 / 1.0	47.9 / 49.5
13	1.165481238	1.8 / 1.2	**97.1 / 98.3**	1.0 / 0.4
14	1.176935519	**51.4 / 49.6**	0.4 / 0.4	48.2 / 50.0

Table 2. Strain/Kinetic(S/K) energy distributions of the crystal plate at each resonance with five vibration modes with $c_{15} = c_{51} = 10^{-5}$.

Mode Number	Normalized Frequency	Extension (S/K %)	Flexural (S/K %)	Face-shear (S/K %)	**Thickness-shear** (S/K %)	Thickness-twist (S/K %)
1	0.916938345	0 / 0	**80.6 / 88.7**	0.2 / 0.4	19.3 / 10.9	0 / 0
2	0.971552057	0 / 0	**77.6 / 80.2**	1.5 / 5.6	20.8 / 14.2	0 / 0
3	0.979178492	0 / 0	16 / 5	**79.3 / 94.1**	4.6 / 0.9	0 / 0
4	0.993080257	**97.4 / 99.5**	0 / 0	0 / 0	0 / 0	2.6 / 0.5
5	1.001670439	0 / 0	1.3 / 1.1	0 / 0	**98.7 / 98.9**	0 / 0
6	1.013299571	0 / 0	19.9 / 17.1	0 / 0.1	**80.1 / 82.8**	0 / 0
7	1.025555986	0 / 0	**55.9 / 53.3**	0.1 / 0.3	44 / 46.4	0 / 0
8	1.044587269	0 / 0	27.9 / 24.1	0 / 0.1	**72.1 / 75.8**	0 / 0
9	1.070274472	0 / 0	43 / 32.1	11 / 28	**46 / 39.8**	0 / 0
10	1.072759691	0 / 0	18.4 / 8.7	**45.2 / 71.1**	36.4 / 20.2	0 / 0
11	1.092467492	0 / 0	**51.1 / 46.8**	0.2 / 0.6	48.6 / 52.6	0 / 0
12	1.097295681	**95.9 / 99**	0 / 0	0 / 0	0 / 0	4.1 / 1
13	1.121051898	0 / 0	47.3 / 43	0.1 / 0.1	**52.6 / 56.9**	0 / 0
14	1.147525190	0 / 0	**54.3 / 49.5**	0.4 / 0.9	45.4 / 49.5	0 / 0
15	1.153644170	0.2 / 0.4	0 / 0	0 / 0	0 / 0	**99.8 / 99.6**
16	1.157412751	0.2 / 0.4	0 / 0	0 / 0	0 / 0	**99.8 / 99.6**
17	1.165473144	0 / 0	4.2 / 1.3	**93.9 / 98.3**	1.9 / 0.4	0 / 0
18	1.176678522	0.2 / 0.6	0 / 0	0 / 0	0 / 0	**99.8 / 99.4**
19	1.187020941	0 / 0	**54.2 / 49.5**	0.2 / 0.4	45.6 / 50.1	0 / 0

Table 3. Strain/Kinetic(S/K) energy distribution variations of three vibration modes with five vibration modes with $c_{16} = c_{61} = 10^{-5}$

Mode Number in three modes	Mode Number In five modes	Frequency $(Freq_3\text{-}Freq_5)/Freq_3$ Changes (%)	Flexural $Abs(FL_3\text{-}FL_5)$ (S/K %)	Face-shear $Abs(FS_3\text{-}FS_5)$ (S/K %)	**Thickness-shear $Abs(TSh_3\text{-}TSh_5)$** (S/K %)
1	1	0.030	4.2 / 0	0.2 / 0	3.9 / 0
2	2	0.025	**5.1** / 0.4	2.1 / 0.4	3.1 / 0
3	3	0.002	**7.9** / 0.4	**9.7** / 0.4	1.7 / 0
4	5	0.001	0.1 / 0.1	0 / 0	0.1 / 0.1
5	6	0.006	0.6 / 0.3	0.1 / 0	0.5 / 0.3
6	7	0.017	2.0 / 0.1	0.2 / 0	1.8 / 0.1
7	8	0.012	0.7 / 0.2	0.1 / 0	0.5 / 0.2
8	9	0.012	**7.6** / 1	**13.3** / 2.7	**5.7** / 1.6
9	10	0.005	**6** / 1	**17.2** / 2.7	**11.2** / 1.7
10	11	0.020	2.2 / 0.1	0.3 / 0	2.1 / 0.1
11	13	0.019	2.1 / 0	0.1 / 0	2 / 0.1
12	14	0.022	3.0 / 0	0.4 / 0.1	2.5 / 0
13	17	0.001	2.4 / 0.1	3.2 / 0	0.9 / 0
14	19	0.022	2.8 / 0.1	0.2 / 0	2.6 / 0.1

As the three-mode model has been verified in previous work [9], with Table 1 we can compare the data of the five-mode model with artificial factors of $c_{16} = c_{61} = 10^{-5}$. By excluding the frequency points of the TT and EX modes, we compared the values of the left three vibration modes. We can see from the Table 3 that the variations of artificial factors brought in are: 1) the frequency changes slightly if the value is less than 10^{-3}; 2) energy distribution varies comparatively larger at some frequency points whose value reach more than 5% but does not affect much on the identification of the working mode; 3) the results of kinetic energy varies less than the strain energy with the artificial factors.

In summary, it is clear that the introduction of small artificial constants has enabled the couplings of separated vibration modes. Then the two equations for separated processing are merged and the same solutions are presented through just one solution process with good accuracy. It shows the analytical procedure can be simplified without doing any modification and reconfiguration for the problem. This is important because if all vibration modes can be linked to one enlarged equation, then the procedure will be simpler and reliable. Afterwards, the ode identification can be done with energy procedure we proposed without worrying about profiling costs. Since the results are identical with two separated equations, it is natural to try other separated vibrations in one equation as shown in this study to simplify the analytical process based on artificial coupling.

4. Conclusions

In this paper, we have introduced the artificial factors in the equations of motion of an AT-cut quartz crystal plate with the first-order Mindlin plate theory and managed to enable the two groups of equations with the five vibration modes coupled together. The frequency spectra and dispersion relations of the first-order Mindlin plate theory are obtained and compared. Then the energies of modes and their distributions are calculated and listed in the tables for comparison and examination. The energy identification procedure for the five- mode model can not only identify the FS, FL, and TSh modes but also the TT and EX modes. The coupling relations of modes can be clearly distinguished from the energy distribution from the Table 2 as the separated modes always approach to zero at the specific frequency point. The results of the artificially coupled model have certain changes when compared with the three-mode model at the corresponding points as shown in Table 3. The prediction by the kinetic energy is comparatively stable than the strain energy and is much closer to the original model.

With the replacements by small numbers of certain zeros in elastic constants, we have successfully obtained the artificially coupled five-mode equations of the first-order Mindlin plate theory. The five-modes coupling model provides more modal identification options then the traditional models of three and two modes in two equations. The energy solution is now applicable to all the mode couplings of the first-order Mindlin plate theory of AT-cut quartz crystal plates. The energy distributions of the five-mode model are reasonable accurate and can be used for mode identification without going through the plotting and visual examination. The artificial coupling approach can recapitulate the first-order Mindlin plate equations and obtain reliable facts for mode identification. This approach unified the calculation procedure for energy solution in identifying the modes with potential implementation with computer codes including the finite element analysis for the automation of the vibration mode identification which has been done with mode shape plotting through visual recognition.

Furthermore, it is to be explored that the known modes of vibrations of typical structural components such as beams, rods, and plates with typical forms like extension, flexure, and torsion are studied separately before can now be considered as coupled vibrations for analysis with the same procedure and analytical code artificially. The identification of these coupled vibration modes can be done with the energy method presented in this study. The research direction presented in this study points to the full and coupled vibrations of structural components in a broad frequency range with large number of vibration modes through natural and artificial couplings to streamline and simplify the analytical procedure which is separated in earlier studies.

Author Contributions

Qi Huang is responsible for the analysis and manuscript preparation; Rongxing Wu contributed to the theoretical validation and manuscript improvement; Longtao Xie checked the formulation; Jianke Du checked the results and manuscript; Ji Wang provided the method of the study and guidance through discussions and manuscript editing.The manuscript was prepared with contributions of all authors. All authors discussed the method, formulation, results and reviewed and approved the final version of the manuscript.

Acknowledgments

This work is supported by the National Natural Science Foundation of China (Grant Nos. 11672142 and 11772163), and the K. C. Wong Magana Fund through Ningbo University. Additional funding are from the Research Project Fund of Zhejiang Department of Education (Grant Nos. Y201636501, Y201636745, and Y201738413) and the National Key R&D Program of China (Project 2017YFB1102900) and the Technology Innovation 2025 Program of the City of Ningbo (Grant 2019B10122).

Conflict of Interest

The authors declared no potential conflicts of interest with respect to the research, authorship, and publication of this article.

Funding

1) National Natural Science Foundation of China (Grant Nos. 11672142 and 11772163)
2) K. C. Magana Fund through Ningbo University
3) Research Project Fund of Zhejiang Department of Education (Grant Nos. Y201636501, Y201636745, and Y201738413)
4) National Key R&D Program of China (Project 2017YFB1102900)
5) Technology Innovation 2025 Program of the City of Ningbo (Grant 2019B10122)

References

[1] Parthasarathy, S., Pancholy, M., and Chhapgar, A. F., Piezo-electric Oscillations of Quartz Plates at Even and Half-odd Harmonics, *Nature*, 171(4344), 1953, 216-217.
[2] Parthasarathy, S. and Singh, H., Amplitude of a Quartz Plate vibrating in Liquids, *Nature*, 181(4604), 1958, 260-260.
[3] Mindlin, R. D., Yang, J., (Ed.) *An Introduction to the Mathematical Theory of Vibrations of Elastic Plates*, World Scientific, Hackensack, NJ, 2006.
[4] Mindlin, R. D., Coupled Piezoelectric Vibrations of Quartz Plates, *International Journal of Solids and Structures*, 10(4), 1974, 453-459.
[5] Lee, P. C. Y., An Accurate Two-Dimensional Theory of Vibrations of Isotropic, elastic plates, *Acta Mechanica Solida Sinica*, 24(2), 2011, 125-134.

[6] Yong, Y. K., Wang, J., and Imai, T., On The Accuracy of Mindlin Plate Predictions for the Frequency-Temperature Behavior of Resonant Modes in AT- and SC-cut Quartz Plates, *IEEE Transactions on Ultrasonics, Ferroelectrics, and Frequency Control*, 46(1), 1999, 1-13.
[7] Wang, J. and Momosaki, E., The Piezoelectrically Forced Vibrations of AT-cut Quartz Strip Resonators, *Journal of Applied Physics*, 81(4), 1997, 1868-1876.
[8] Wang, J. and Zhao, W., The Determination of the Optimal Length of Crystal Blanks in Quartz Crystal Resonators, *IEEE Transactions on Ultrasonics, Ferroelectrics, and Frequency Control*, 52(11), 2005, 2023-2030.
[9] Lee, P. C. Y. and Yong, Y. K., Frequency-temperature Behavior of Thickness Vibrations of Doubly-Rotated Quartz Plates affected by Plate Dimensions and Orientations, *Journal of Applied Physics*, 60(7), 1986, 2327-2342.
[10] Mindlin, R. D. and Spencer, W. J., Anharmonic, Thickness-Twist Overtones of Thickness-Shear and Flexural Vibrations of Rectangular, AT-cut, Quartz Plates, *Journal of The Acoustical Society of America*, 42(6), 1967, 1268-1277.
[11] Hu, Y., Cui, Z., Jiang, S., and Yang, J., Thickness-shear Vibration of Circular Crystal Plate in Cylindrical Shell as Pressure Sensor, *Applied Mathematics and Mechanics*, 27(6), 2006, 749-755.
[12] Zhao, Z., Qian, Z., Wang, B., and Yang, J., Analysis of Thickness-shear and Thickness-twist Modes of AT-cut Quartz Acoustic Wave Resonator and Filter, *Applied Mathematics and Mechanics*, 36(12), 2015, 1527-1538.
[13] Wang, J., Wang, Y., Hu, W., Zhao, W., Du, J., and Huang, D., Parallel Finite Element Analysis of High Frequency Vibrations of Quartz Crystal Resonators on Linux Cluster, *Acta Mechanica Solida Sinica*, 21(6), 2008, 549-554.
[14] Yong, Y., Stewart, J. T., Detaint, J., Zarka, A., Capelle, B., and Zheng, Y., Thickness-shear Mode Shapes and Mass-Frequency Influence Surface of a Circular and Electroded AT-cut Quartz Resonator, *IEEE Transactions on Ultrasonics, Ferroelectrics, and Frequency Control*, 39(5), 1992, 609-617.
[15] Zargaripoor, A., Daneshmehr, A. R., and Nikkhah Bahrami, M., Study on Free Vibration and Wave Power Reflection in Functionally Graded Rectangular Plates using Wave Propagation Approach, *Journal of Applied and Computational Mechanics*, 5(1), 2019, 77-90.
[16] Shukla, S. K., Gupta, A., and Sivakugan, N., Analysis of Circular Elastic Plate Resting on Pasternak Foundation by Strain Energy Approach, *Geotechnical and Geological Engineering*, 29(4), 2011, 613-618.
[17] Lee, E. T. and Eun, H. C., Damage Identification Based on the Proper Orthogonal Mode Energy Curvature, *Journal of Vibration and Acoustics*, 137(4), 2015.
[18] Berger, J. B., Wadley, H. N. G., and McMeeking, R. M., Mechanical Metamaterials at the Theoretical Limit of Isotropic Elastic Stiffness, *Nature*, 543(7646), 2017, 533-537.
[19] Huang, Q., Wang, J., Wu, R., Xie, L., and Du, J., Using Kinetic and Strain Energies of Mindlin Plates for Vibration Mode Identification, *Piezoelectricity, Acoustic Waves, and Device Applications,* Chengdu, Sichuan, China, 471-475, 2017.
[20] Wang, J. and Yang, J., Higher-order Theories of Piezoelectric Plates and Applications, *Applied Mechanics Reviews*, 53(4), 2000, 87-99.
[21] Wang, J., Yong, Y. K., and Imai, T., Finite Element Analysis of the Piezoelectric Vibrations of Quartz Plate Resonators with Higher-order Plate Theory, *International Journal of Solids and Structures*, 36(15), 1999, 2303-2319.
[22] Wang, J., Yu, J. D., Yong, Y. K., and Imai, T., A Finite Element Analysis of Frequency–temperature Relations of AT-cut Quartz Crystal Resonators with Higher-order Mindlin Plate Theory, *Acta Mechanica*, 199(1-4), 2008, 117-130.
[23] Yasir, R. Y., Al-Muslimawi, A. H., and Jassim, B. K., Numerical Simulation of Non-Newtonian Inelastic Flows in Channel based on Artificial Compressibility Method, *Journal of Applied and Computational Mechanics*, 6(2), 2020, 271-283.
[24] Bechmann, R., Elastic and Piezoelectric Constants of Alpha-Quartz, *Physical Review*, 110(5), 1958, 1060-1061.
[25] Wang, J., Zhao, W., and Bian, T., A Fast Analysis of Vibrations of Crystal Plates for Resonator Design Applications, *2004 IEEE International Frequency Control Symposium and Exposition*, Montreal, Canada, 596-599, 2004.
[26] Wu, R. *et al.*, Free and Forced Vibrations of SC-cut Quartz Crystal Rectangular Plates with the First-order Mindlin Plate Equations, *Ultrasonics*, 73, 2016, 96-106.

ORCID iD

Qi Huang https://orcid.org/0000-0001-9557-9649
Rongxing Wu https://orcid.org/0000-0003-1401-0544
Longtao Xie https://orcid.org/0000-0002-6791-5411
Ji Wang https://orcid.org/0000-0002-0724-7538

How to cite this article: Huang Q., Wu R., Xie L., Du J., Wang J. The Integrated Analysis of Vibrations of Quartz Crystal Plates through Artificial Coupling Factors, *J. Appl. Comput. Mech.*, 7(1), 2021, 69–77. https://doi.org/10.22055/JACM.2020.34730.2470